Aalto University

OPEN ACCESS

This is an electronic reprint of the original article.
This reprint may differ from the original in pagination and typographic detail.

Rontu, Ville; Selent, Anne; Zhivonitko, Vladimir V.; Scotti, Gianmario; Koptyug, Igor V.; Telkki, Ville-Veikko; Franssila, Sami

Efficient Catalytic Microreactors with Atomic-Layer-Deposited Platinum Nanoparticles on Oxide Support

Published in:
CHEMISTRY: A EUROPEAN JOURNAL

DOI:
10.1002/chem.201703391

Published: 01/01/2017

Document Version
Other version

Published under the following license:
CC BY-NC

Please cite the original version:
Rontu, V., Selent, A., Zhivonitko, V. V., Scotti, G., Koptyug, I. V., Telkki, V-V., & Franssila, S. (2017). Efficient Catalytic Microreactors with Atomic-Layer-Deposited Platinum Nanoparticles on Oxide Support. *CHEMISTRY: A EUROPEAN JOURNAL*, *23*, 16835 – 16842. https://doi.org/10.1002/chem.201703391

This material is protected by copyright and other intellectual property rights, and duplication or sale of all or part of any of the repository collections is not permitted, except that material may be duplicated by you for your research use or educational purposes in electronic or print form. You must obtain permission for any other use. Electronic or print copies may not be offered, whether for sale or otherwise to anyone who is not an authorised user.

Supporting information

1. Microreactor fabrication

The 1 x 4 cm microreactor chips consist of 36 parallel channels of 50 µm width, 100 µm depth and either 5, 10 or 20 mm length connected to 200 x 100 µm inlet and outlet channels by perpendicular 200 x 100 µm channels. We used thermally oxidized, 300 µm thick, double side polished <100> silicon wafers (Figure S1a). The SiO_2 thickness was 600 nm. The oxide on the topside was patterned by photolithography and wet etching in buffered hydrogen fluoride (Figure S1b). The SiO_2 pattern was used as a mask for deep reactive ion plasma etching (DRIE) to form the microchannels of the microreactor (Figure S1c). The DRIE process was done in an Oxford Plasmalab 100 cryogenic etcher, using a SF_6/O_2 chemistry. On the backside 100 nm of aluminum was sputtered using Oxford Plasmalab 400 and patterned by photolithography and wet etching in phosphoric acid (Figure S1d). The aluminum layer was used as a hard mask for a DRIE step to create 500 µm diameter inlet and outlet holes. After this 20 µm wide diamond dicing saw blades were used to dice the wafer into chips consisting of 2-4 microreactors. Aluminum and SiO_2 layers were removed in 1:10 HF solution (Figure S1e). Catalyst support and catalyst were then deposited on the chips by ALD. After catalyst deposition chips were capped with a 125 µm thick commercial laminating foil (Fellowes Laminating Pouches, see Figure S1f), which is composed of three layers: 75 µm polyethylene terephthalate (PET), 25 µm ethylene-vinyl acetate (EVA), and 25 µm low-density polyethylene (LDPE). The LDPE layer was turned towards the channels. Capping procedure consists of the following steps:

- A thin (~500 µm) graphite disc was placed on a hotplate.
- The laminating foil was placed on the graphite disc with the LDPE layer facing upwards.
- The wafer was placed on the laminating foil with the channel side at the bottom, contacting it with the laminating foil.
- A planar object (in our case a pile of 10 dummy silicon wafers) was placed on the wafer and a weight on top of the planar object. The weight was 4 kg for a 100 mm wafer. Larger wafers would require a higher weight, in proportion to wafer area.
- The temperature of the hotplate was ramped up to 120 °C. When the temperature was reached, the wafer was kept on the hotplate for an additional 5 minutes.

Following the capping the chips were diced into single microreactors.

Initially we attempted to cap the microreactors with glass wafers using anodic bonding. However, Pt nanoparticles were deposited on all surfaces on the wafer. Pt nanoparticles on the bonding surface led to poor bonding. Even when the initial results looked good, there was gradual debonding on the time scale

of few hours. To fabricate microreactors for high temperatures, removal of Pt nanoparticles from bonding areas is required to allow anodic bonding with glass wafer.

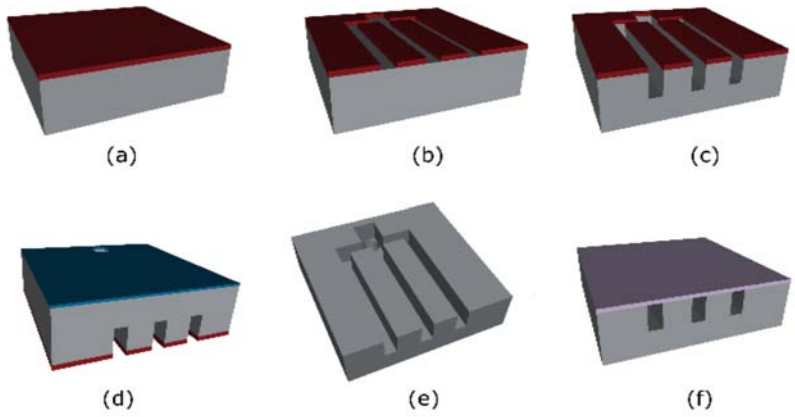

Figure S1. Microreactor fabrication process steps. See text for details.

2. TEM and SEM image processing and particle size analysis

Raw TEM and SEM images were processed in Fiji image processing software. First the image (Figure S2 a) type was changed from 16 bit to 8 bit. Following this background was removed using *Subtract background* tool using *Rolling ball* algorithm (Figure S2 b). After subtracting background brightness and contrast was adjusted with *B & C auto* tool (Figure S2 c). *Gaussian blur* was used blend adjacent pixels creating continuous coloring (Figure S2 d). Finally, images were thresholded using *Auto threshold* tool (Figure S2 e). Threshold using geometric *Triangle* algorithm gave appropriate result for TEM images while *Default* algorithm gave best results for SEM images. *Watershed* tool was used to separate interconnected particles (Figure S2 f).

Particle analysis was performed using *Analyze particles* tool in Fiji. For particle size analysis, particles at image edges were excluded as well as particles smaller than 0.5 nm and with circularity smaller than 0.7 as they were thought to be artifacts from image processing. Figure S2 e) shows particles that remained after filtering. For particle surface coverage analysis, particles at edges were included.

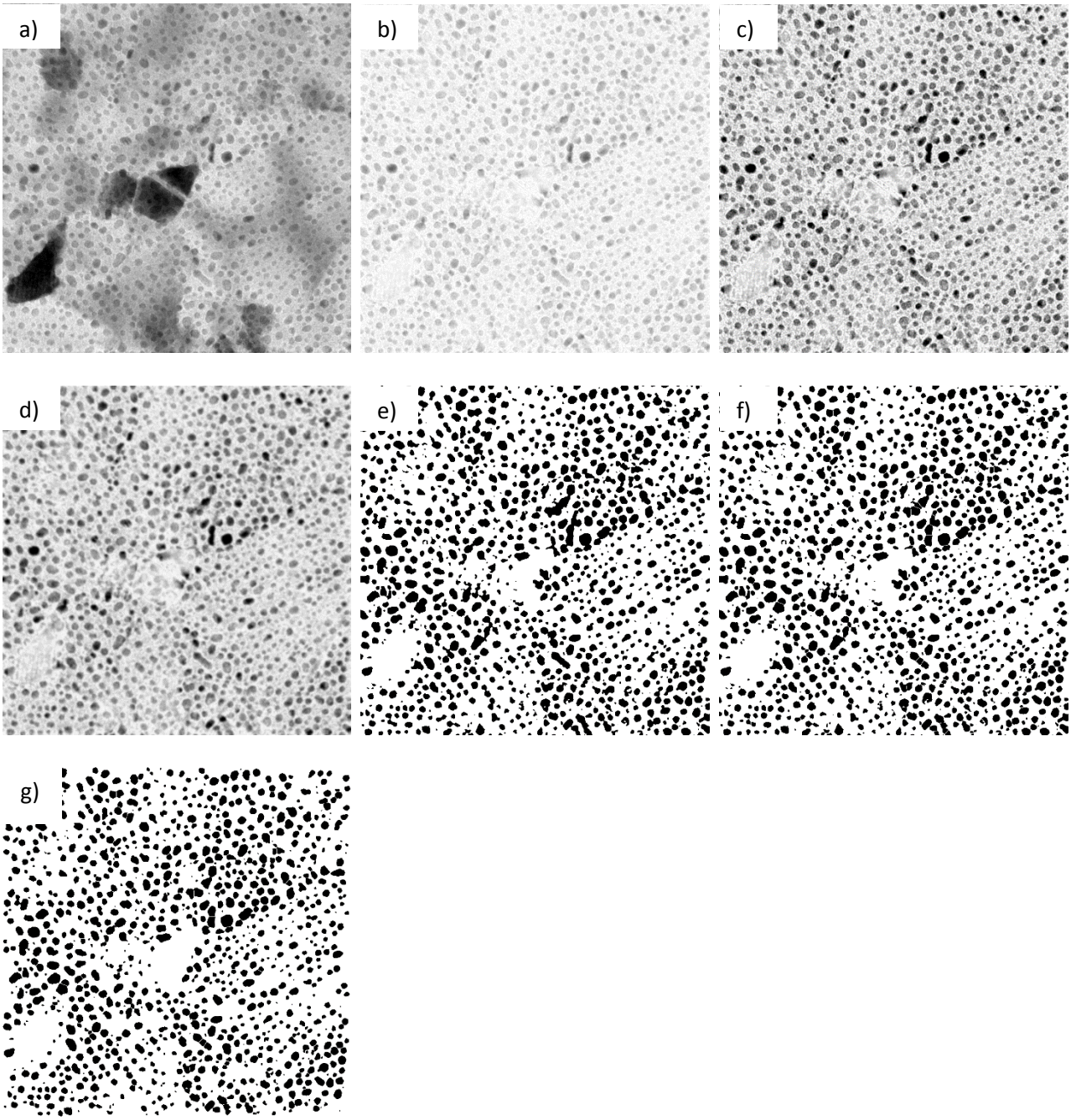

Figure S2. Image processing steps shown for 40 cycles of Pt on 20 nm TiO_2: a) starting image, b) background subtracted, c) brightness and contrast corrected, d) Gaussian blur applied, e) threshold applied, f) Watershed applied and e) artefacts filtered showing only particles that were used for particle size analysis.

3. RD TOF NMR imaging

The pulse sequence of 2D yz encoded RD TOF NMR experiment is shown in Fig. S3. It comprises two parts: First, the position of the molecules inside the chip is encoded in the spin coherences by the use of gradients. This procedure is similar to phase encoding in a conventional magnetic resonance imaging experiment. Thereafter the information is stored by flipping the magnetization to z-axis. As a result, only

T_1 relaxation affects the magnetization and the information is saved for the short travel time between the encoding and detection coils. The information is then read out by a train of detection coil 90° pulses.

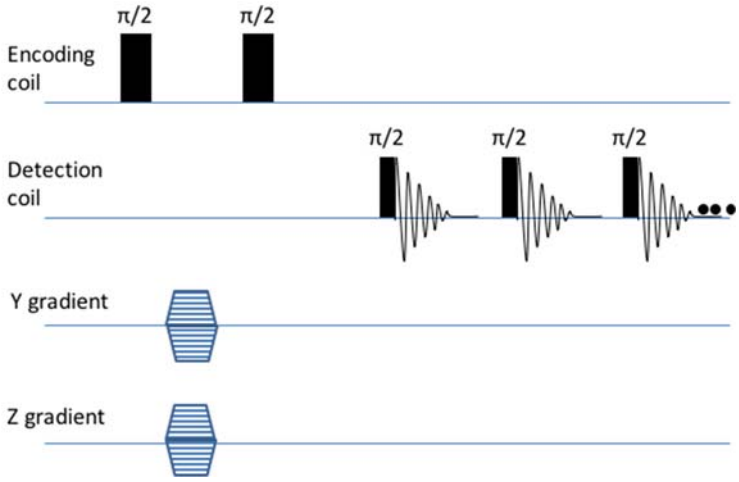

Figure S3. The pulse sequence of YZ- encoded time-of-flight RD NMR pulse sequence.

The total length of the trapezoidal gradient pulse was 250 μs (ramp time 50 μs) and the delay between the two 90° encoding pulses was 400 μs. The number of FIDs collected during one scan was 60 and the number of accumulated scans was 64. The number of complex points collected in each FID was 256, and the time resolution (acquisition time of one FID plus a 3 ms additional delay) was 24 ms. The total experimental time was 1 h 40 min. The lengths of the detection and encoding π/2 pulses were 2.5 μs (18 dB) and 100 μs (-6 dB), respectively. The field of View (FOV) was 8 mm in the y direction and 35 mm in the z direction. The resolution in the z and y directions was 2.2 and 1 mm, respectively (with 16 and 8 phase encoding steps). The TOF images were processed in MATLAB using CH_3 group signal of propene. The number of points in each image dimension was doubled by zero filling before the Fourier transform.

4. Activity of the chips based on the first order kinetics

The chemical process of propene hydrogenation:

$$C_3H_6 + H_2 = C_3H_8. \quad (1)$$

If the order of the reaction between propene and hydrogen over TiO_2-supported platinum is assumed to be first and zero with respect to hydrogen and propylene, respectively, which has been shown to be approximately true for pumice-supported rhodium,[1] the rate of the reaction, *r*, in a small volume of the reactor *dV* is

$$r = \frac{d[C_3H_8]}{dt} = k[H_2]^1[C_3H_8]^0 = k[H_2], \quad (2)$$

[1] R. S. Mann, T. R. Lien, *J. Catal*. 1969, 15, 1-7

where [*C*] is the concentration of substance *C* and *k* is the rate constant of the reaction in the small volume *dV*.

In the hydrogenation of propene under continuous flow conditions

$$[H_2] = \frac{F_{H_2}}{\nu}, \tag{3}$$

where F_{H_2} is the rate of flow (mol s^{-1}) of hydrogen and ν is the volumetric flow rate (m^3 s^{-1}) though the reactor cross-section. Because the initial hydrogen:propene ratio was 3:1,

$$F^0_{H_2} = 3F^0_{C_3H_6}, \tag{4}$$

where $F^0_{H_2}$ and $F^0_{C_3H_6}$ are input rate of flow for hydrogen and propene, respectively. Taking this into account, the generation (reaction) rate can be expressed as

$$r = \frac{k}{\nu}F_{H_2} = \frac{k}{\nu}\left(3F^0_{C_3H_6} - F_{C_3H_8}\right) = \frac{kF^0_{C_3H_6}}{\nu}(3 - \mathcal{X}), \tag{5}$$

where $F_{C_3H_8}$ is the rate of flow for propane produced in the reactor and $\mathcal{X}$ is the conversion of propene, or alternatively the reaction yield of propane. Assuming all gases as ideal ones and taking into account the change in the number of molecules in the reaction, the volumetric flow rate is equal to $\nu = \nu_0(1 - \mathcal{X}/4)$. Therefore, the reaction rate is expressed as

$$r = \frac{kF^0_{C_3H_6}}{\nu_0}\frac{(3-\mathcal{X})}{(1-\mathcal{X}/4)}, \tag{6}$$

Then, taking into account the differential form for the mass balance in ideal PFR reactor,[2]

$$\frac{d\mathcal{X}}{dV} = \frac{r}{F^0_{C_3H_6}}, \tag{7}$$

the integration by the whole reactor volume (V_R) leaves us with the following equation

$$V_R = \frac{\nu_0}{k}\left(\frac{\mathcal{X}}{4} + \frac{3}{4}\ln\left[1 - \frac{\mathcal{X}}{3}\right] + \ln\left[\frac{3}{3-\mathcal{X}}\right]\right), \tag{8.1}$$

or alternatively

$$l_R = \frac{u_0}{k}\left(\frac{\mathcal{X}}{4} + \frac{3}{4}\ln\left[1 - \frac{\mathcal{X}}{3}\right] + \ln\left[\frac{3}{3-\mathcal{X}}\right]\right), \tag{8.2}$$

[2]Fogler, H. S. *Elements of chemical reaction engineering*; Pearson international ed., 4th ed. ed.; Pearson Education International: Upper Saddle River, N.J., 2006.

where l_R (m) is the reactor length and u_0 is the linear flow velocity (m s^{-1}). Eq. (8.2) was used for determination of k values by using parameters determined in RD NMR experiments. Moreover, we can use this equation to determine the specific catalytic activity using the standard definition for continuous flow reactors

$$A = \frac{F^0_{C_3H_6}\mathcal{X}}{A_{Pt}}, \tag{9}$$

where *A* is the activity (mol $s^{-1}m^{-2}$) and A_{Pt} is area of exposed Pt surface in the reactor (m^2). This equation is valid only when $\mathcal{X} \ll 1$. Thus, in order to use it for our microreactors we need to fulfill somehow this condition. To do it we can model such a length of the reactor (l_R) that the reaction yield is low ($\mathcal{X}'$). As the specific activity is independent from the reactor length, such modelling will provide the correct values of *A*. The exposed Pt surface in the modeled reactor of length l_R will be

$$a_{Pt} = \frac{l_R}{L_R}A_{Pt}, \tag{10}$$

where L_R is the length of the reactor which was used in practice, and gave large reaction yield. Then, the specific activity will be

$$A = \frac{F^0_{C_3H_6}L_R\mathcal{X}'}{l_R A_{Pt}} = \frac{kF^0_{C_3H_6}L_R\mathcal{X}'}{u_0 A_{Pt}} / (\frac{\mathcal{X}'}{4} + \frac{3}{4}\ln[1 - \frac{\mathcal{X}'}{3}] + \ln[\frac{3}{3-\mathcal{X}'}]). \tag{11}$$

Eventually we seek the limit of A from the Eq. (11) for $\mathcal{X}' \to 0$:

$$A = \lim_{\mathcal{X}'\to 0}(\frac{kF^0_{C_3H_6}L_R\mathcal{X}'}{u_0 A_{Pt}} / (\frac{\mathcal{X}'}{4} + \frac{3}{4}\ln[1 - \frac{\mathcal{X}'}{3}] + \ln[\frac{3}{3-\mathcal{X}'}])) = \frac{3kF^0_{C_3H_6}L_R}{u_0 A_{Pt}} = \frac{kF^0_{H_2}L_R}{u_0 A_{Pt}} = \frac{k[H_2]_0 V_R}{A_{Pt}}. \tag{12}$$

This equation is used to determine specific activities from the k values determined from RD NMR experiments. We note that the same equation can be obtained in a different way by saying that the specific activity is the initial reaction rate ($k[H_2]_0$) related to the concentration of the catalyst sites in the reactor $[cat] = A_{Pt}/V_R$. Thus, $k[H_2]_0/[cat]$ provides the same result as in Eq. 12, but in a more intuitive way. Finally, it was convenient for calculations to present Eq. 12 in the form of

$$A = \frac{k[H_2]_0 V_R}{A_{Pt}} = \frac{3PV_R k}{4RTA_{Pt}}. \tag{13}$$

Here, *k* is the rate constant of the reaction calculated by Eq. (8.2) and A_{Pt} (see Table 2) is determined from

$$A_{Pt} = 2S_c A_s, \quad (14)$$

where the Pt particles on the channel surfaces were assumed to be half-spherical, A_s is the total surface area of the channels covered by the catalyst and S_c is the surface coverage shown in Table 1. P is the total pressure of the gas mixture, and factor ¾ in Eq. (13) takes into account the partial pressure of H_2 in the gas mixture, R is the universal gas constant, T is the temperature and V_R is the volume of the microfluidic chip, which is $2.3 \cdot 10^{-9}$ m^3 for the 10 mm reactor and $3.8 \cdot 10^{-9}$ m^3 for the 20 mm reactor.

Table S1. The total surface area of the channels covered by the catalyst.

	Reaction channel length, L_R (mm)	**Surface area, A_s (mm^2)**
TiO_2	5	71
	10	112
	20	194
PirSi	20	134